SCIENTIFIC REPORTS
nature research

OPEN

Designing of Carbon Nitride Supported $ZnCo_2O_4$ Hybrid Electrode for High-Performance Energy Storage Applications

Meenu Sharma & Anurag Gaur*

This study reports a unique graphitic-C_3N_4 supported $ZnCo_2O_4$ composite, synthesized through a facile hydrothermal method to enhance the electrochemical performance of the electrode. The g-C_3N_4@$ZnCo_2O_4$ hybrid composite based electrode exhibits a significant increase in specific surface area and maximum specific capacity of 157 mAhg^{-1} at 4 Ag^{-1}. Moreover, g-C_3N_4@$ZnCo_2O_4$ electrode maintained significant capacity retention of 90% up to 2500 cycles. Utilizing this composite in the development of the symmetric device, g-C_3N_4@$ZnCo_2O_4$//g-C_3N_4@$ZnCo_2O_4$ displays a specific capacity of 121 mAhg^{-1}. The device exhibits an energy density of 39 Whkg^{-1} with an equivalent power density of 1478 Wkg^{-1}. A good cycling stability performance with an energy efficiency of 75% and capacity retention of 71% was observed up to 10,000 cycles. The superior performance of g-C_3N_4@$ZnCo_2O_4$ is attributed to the support of the g-C_3N_4 which increases the surface area, electroactive sites and provides chemical stability for electrochemical performance. The outstanding performance of this exclusive device symbolizes remarkable progress in the direction of high-performance energy storage applications.

The need for advanced energy storage devices is in great demand because of numerous portable electronic devices and the emergence of hybrid electric vehicles in modern society. However, most of these new inventions require high-performance energy storage with high energy and power densities[1,2]. Among different energy storage devices, electrochemical capacitors with high power density and batteries with high energy density have gained significant research attention to meet the needs of increasing demand for energy storage applications. Several materials like metal hydroxides/oxides, activated carbon and conducting polymers have been explored as electrodes material for energy storage applications, with an emphasis on exploring new composite to boost the electrochemical efficiency of the energy storage device[3]. Lithium-ion batteries can store high energy up to 150–200 Whkg^{-1}, but confined to low power density and poor cycle life, whereas supercapacitors have high power energy, low cost and low maintenance for high-power delivery applications[4]. Therefore, the fabrication of rationally designed hybrid electrode materials is in highest demand to enhance the electrochemical performance of energy storage applications.

Transition metal oxides with various nanostructures have been used widely for electrode material because of their high theoretical capacitance. In the past years, $ZnCo_2O_4$ has aroused one of the most capable electrode materials by researchers toward their applications for supercapacitors because of their high electrochemical activities and speedy faradic reactions[5]. However, it suffers relatively poor electrical conductivity and a considerable reduction in capacitance during long cycling life and low surface area[6].

Among the various carbon-based nanostructures, graphitic carbon nitride (g-C_3N_4) is a soft polymer with porous nature and sheet-like crystallite has attracted considerable attention due to its highly active nitrogen sites, excellent physical and chemical strength, and low-cost feature[7]. In the application of water splitting, waste-water detoxification, solar cells and supercapacitors, g-C_3N_4 carbon-based materials show superior performance because of its outstanding optical properties, high mechanical strength and thermal conductivity[8]. The nitrogen presence in g-C_3N_4 provides more active sites and advances the capacitance while preserving the cyclability of the electrochemical device[9,10]. Therefore, the composite of g-C_3N_4 and $ZnCo_2O_4$ could have great advancement

Department of Physics, National Institute of Technology, Kurukshetra, 136119, Haryana, India. *email: anuragdph@nitkkr.ac.in

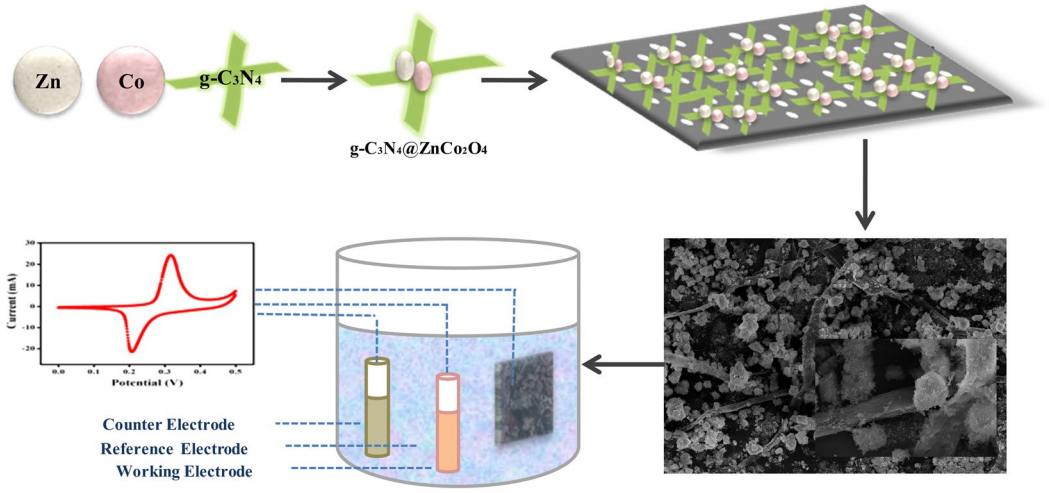

Figure 1. Schematic illustration of g-C_3N_4@$ZnCo_2O_4$ composite mechanism along with the testing of the fabricated electrode.

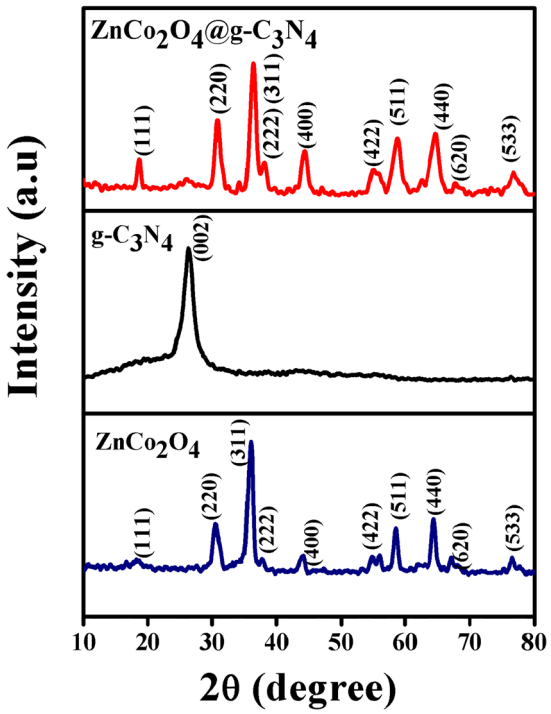

Figure 2. XRD patterns of g-C_3N_4@$ZnCo_2O_4$, $ZnCo_2O_4$ and g-C_3N_4.

in rate capability and specific capacitance[9]. To date, only a few studied of g-C_3N_4 with $Ni(OH)_2$[11,12], MnO_2[13] and $NiCo_2O_4$[14] for energy storage application have been reported.

In this work, we synthesize g-C_3N_4 hybridized $ZnCo_2O_4$ composite for the electrode material in order to develop a high-performance symmetric supercapattery device. This hybrid g-C_3N_4@$ZnCo_2O_4$ composite exhibits excellent electrochemical performance through a specific capacity of 154 $mAhg^{-1}$ at 4 Ag^{-1} with 90% of capacity retention up to 2500 cycles. Further g-C_3N_4@$ZnCo_2O_4$ based solid-state symmetric supercapattery device g-C_3N_4@$ZnCo_2O_4$//g-C_3N_4@$ZnCo_2O_4$ has been assembled, which exhibits a 39 $Whkg^{-1}$ of energy density with an equivalent power density of 1478 Wkg^{-1}.

Results and Discussion

The synthesis of g-C_3N_4@$ZnCo_2O_4$ hybrid composite with high surface area is performed through a simple hydrothermal process. The schematic illustration of g-C_3N_4@$ZnCo_2O_4$ formation mechanism along with the testing of the fabricated electrode is shown in Fig. 1. The obtained g-C_3N_4@$ZnCo_2O_4$ based electrode is incorporated into a solid-state symmetric Supercapattery device, which possesses a favourable energy density and power density.

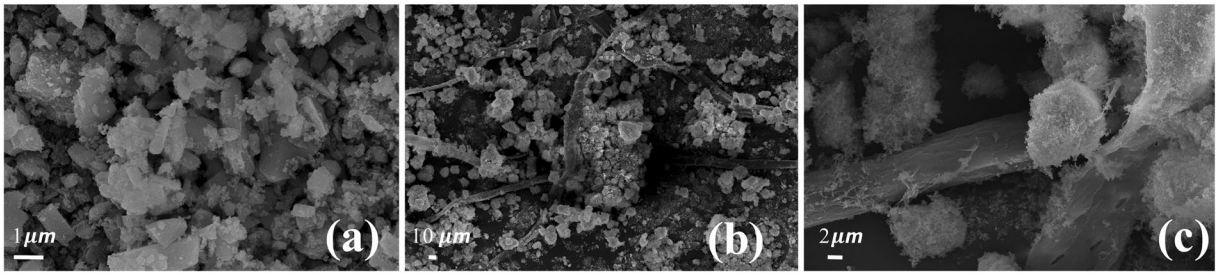

Figure 3. SEM images: (**a**) $ZnCo_2O_4$, (**b**,**c**) g-C_3N_4@$ZnCo_2O_4$ composite.

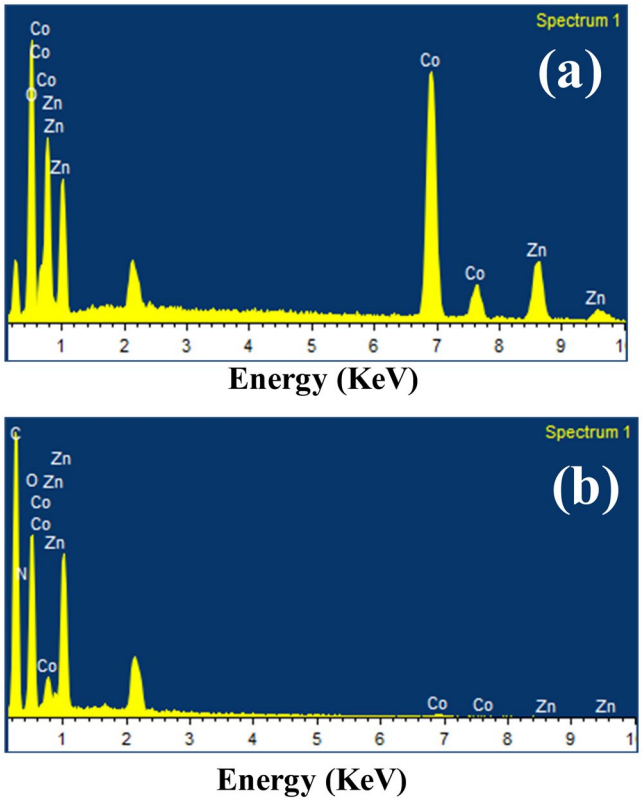

Figure 4. EDX of (**a**) $ZnCo_2O_4$ (**b**) g-C_3N_4@$ZnCo_2O_4$ composite.

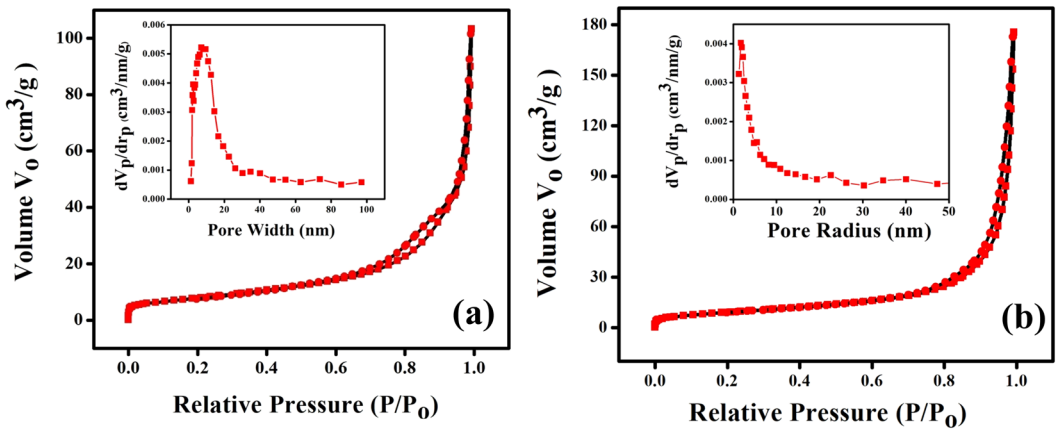

Figure 5. N_2 adsorption/desorption isotherms with corresponding pore size distributions: (**a**) pure $ZnCo_2O_4$ and (**b**) g-C_3N_4@$ZnCo_2O_4$ composite.

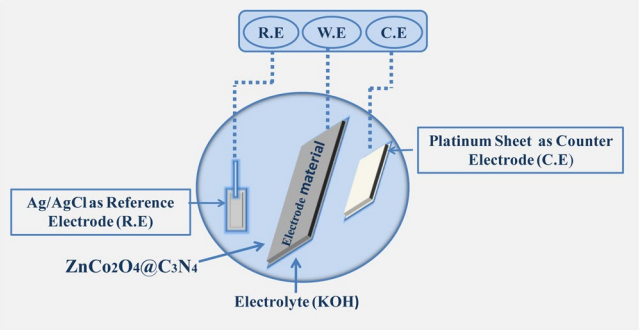

Figure 6. The Schematic illustration of testing a single electrode in the three-electrode electrochemical system.

XRD pattern of g-C_3N_4, $ZnCo_2O_4$ and g-C_3N_4@$ZnCo_2O_4$ is displayed in Fig. 2. For $ZnCo_2O_4$ sample, all the peaks of the XRD patterns are well matched to the (JCPDS No. 14-0117) whereas XRD pattern of g-C_3N_4@$ZnCo_2O_4$ shows the diffraction peaks corresponding to $ZnCo_2O_4$ and g-C_3N_4, implying the good formation of g-C_3N_4@$ZnCo_2O_4$ composites. Figure 3(a) shows the SEM micrographs of pristine $ZnCo_2O_4$ and Fig. 3(b,c) shows the SEM micrographs of g-C_3N_4@$ZnCo_2O_4$ composites at different magnifications. The SEM images of pristine $ZnCo_2O_4$ shows the agglomerate clusters, whereas g-C_3N_4@$ZnCo_2O_4$ composites show clusters with fibres distribution. The visible spaces between clusters could provide a channel for the movement of electrolyte ions and achieve a high specific surface area. Figure 4(a) represents the EDX pattern of $ZnCo_2O_4$ and Co, Zn, and O three kinds of elements are detected, whereas Fig. 4(b) represents the C, N, Co, Zn, and O five kinds of elements for composite g-C_3N_4@$ZnCo_2O_4$.

The evaluation of the specific surface area and porous nature of pristine $ZnCo_2O_4$ and g-C_3N_4@$ZnCo_2O_4$ has been done using the N_2 adsorption-desorption isotherms. Figure 5(a,b) displays the nitrogen adsorption-desorption measurements with inset the BJH pore size distribution plot for pristine $ZnCo_2O_4$ and g-C_3N_4@$ZnCo_2O_4$, respectively. The isotherms of both the samples show IV type behaviour with hysteresis loops, indicating the mesoporous nature. The Specific surface area calculated from the Brunauer-Emmett-Teller (BET) isotherms is 46 m^2g^{-1} for a g-C_3N_4@$ZnCo_2O_4$ sample which significantly greater than the surface area for pristine $ZnCo_2O_4$ (22 m^2g^{-1}). This increase in surface area of g-C_3N_4@$ZnCo_2O_4$ composite could be ascribed to the incorporation of Carbon nitride, which leads to the formation of more numbers of pores[15]. The BJH plot for both the samples displays the pore size within the range of 2 to 50 nm, which shows the mesoporous nature of the samples. The mesoporous nature of the sample could provide effortless access for electrolyte ions with a short diffusion path for electrochemical reactions[16,17].

The electrochemical analysis of fabricated electrodes in a three-electrode configuration is schematically illustrated in Fig. 6. The CV curves of pristine $ZnCo_2O_4$ and g-C_3N_4@$ZnCo_2O_4$ electrodes at a constant scan rate of 20 mVs^{-1} in the potential range of 0.0 to 0.5 V is shown in Fig. 7(a). The CV curve for g-C_3N_4@$ZnCo_2O_4$ shows a very high amplitude of current as compared to $ZnCo_2O_4$ electrode, resulting in an enhancement in the specific Capacity[18]. A pair of redox peaks is primarily raised from faradic redox reactions linked to M-O/M-O-OH (M = Zn or Co)[19,20]. Figure 7(b) demonstrates the CV curves of g-C_3N_4@$ZnCo_2O_4$ at different scan rates from 2–100 mVs^{-1}. The amplification and shift in the position of the anodic and cathodic peak are appeared with the increase of scan rates, indicating the quick and reversible redox responses happening at the electro/electrolyte interface[21,22]. The GCD curves of $ZnCo_2O_4$ and g-C_3N_4@$ZnCo_2O_4$ electrodes at a constant specific current of 4 Ag^{-1} is shown in Fig. S1. Figure 7(c) displays the GCD curves of g-C_3N_4@$ZnCo_2O_4$ at a various specific current of 4, 6, 7 and 8 Ag^{-1}. Figure 7(d) represents the specific discharge capacity of the g-C_3N_4@$ZnCo_2O_4$ electrode evaluated from GCD curves. The maximum specific capacity obtained for the hybrid g-C_3N_4@$ZnCo_2O_4$ electrode is 157 $mAhg^{-1}$ at 4 Ag^{-1}. The superior capacity retention of 90% up to 2500 constant GCD cycles at 10 A g^{-1} is demonstrated by the g-C_3N_4@$ZnCo_2O_4$ based single electrode.

We further assembled the symmetric devices, referred to supercapattery, based on g-C_3N_4@$ZnCo_2O_4$ electrodes having sandwiched construction of g-C_3N_4@$ZnCo_2O_4$//gel electrolyte//g-C_3N_4@$ZnCo_2O_4$ as shown in Fig. 8. This configuration of the symmetric device with the gel electrolyte not only prevents the leakage of aqueous electrolyte but also expand the potential window[23,24]. The optimization of a suitable operating potential window is an important assignment for supercapattery device to sustain the electroactivity of working electrodes and electrolyte[25]. So, initially CV measurements were performed at the different operating potential window as shown in Fig. 9(a). The potential window from 0 to 1.5 V is found to be constant for the assembled supercapattery device which is higher than the symmetric device in liquid electrolytes[26,27].

Figure 9(b) displays the CV curves of the electrodes between 0.0–1.5 V at a different scan rate of 5, 10, 20, and 50 mVs^{-1}, respectively. The similarity in CV curves of the device with increasing scan rates indicates the excellent rate capability of the device[28,29]. The GCD measurements at a specific current of 4.6, 5.9, 7.2 and 8.5 Ag^{-1} is shown in Fig. 9(c) within the potential window of 0 to 1.5 V. By using these GCD curves, the specific discharge capacity (Q_s) is calculated and plotted as a function of specific current in Fig. 9(d). The Q_s values calculated from GCD curves of the symmetric device are 121, 100, 96 and 89 $mAhg^{-1}$ for 4.6, 5.9, 7.2 and 8.5 Ag^{-1}, respectively. To estimate the overall efficiency of the assembled symmetric device, energy and power density were calculated and illustrated as a Ragone plot in Fig. 10(a). This device achieved a maximum energy density of 39 $Whkg^{-1}$ at a power density of 1478 Wkg^{-1}. The g-C_3N_4@$ZnCo_2O_4$//gel electrolyte//g-C_3N_4@$ZnCo_2O_4$ symmetric device

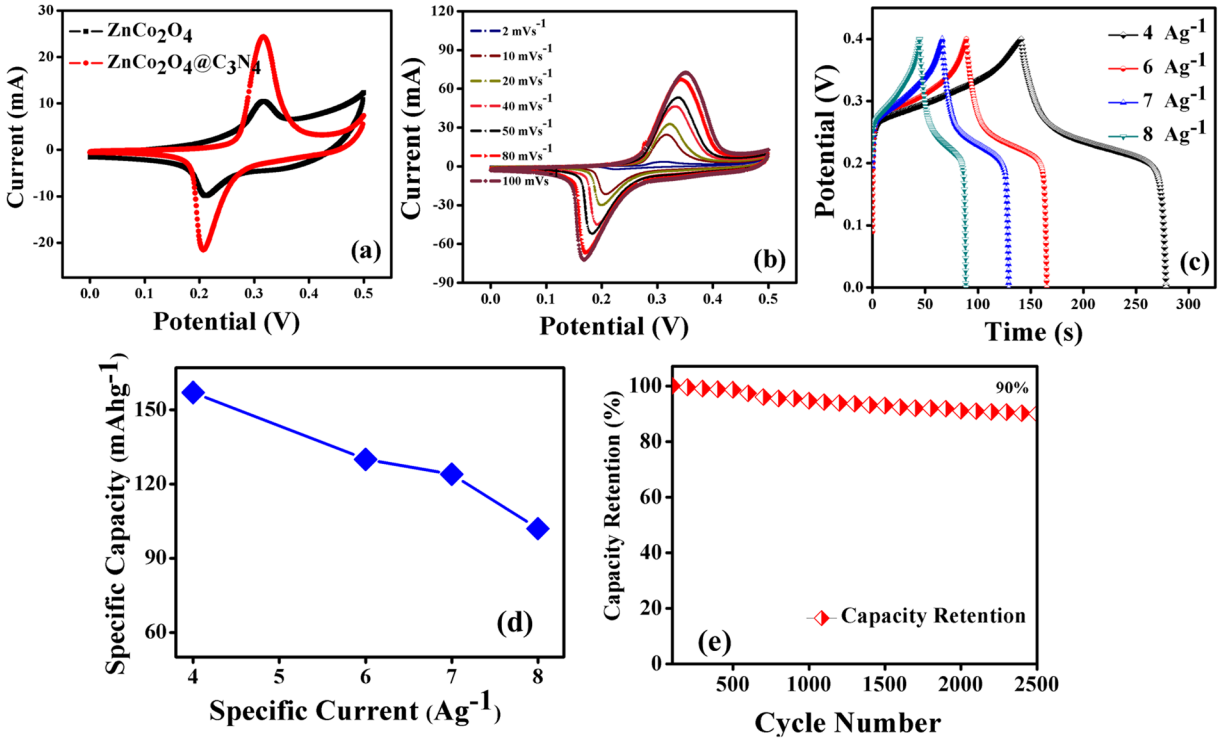

Figure 7. (**a**) CV curves of $ZnCo_2O_4$ and g-C_3N_4@$ZnCo_2O_4$ at a constant scan rate of 20 mVs^{-1}. (**b**) CV curves for g-C_3N_4@$ZnCo_2O_4$ for different scan rates. (**c**) GCD curves for g-C_3N_4@$ZnCo_2O_4$ at different specific current. (**d**) Specific Capacity as a function of specific current for g-C_3N_4@$ZnCo_2O_4$ sample. (**e**) Capacity retention up to 2500 cycles for g-C_3N_4@$ZnCo_2O_4$ sample.

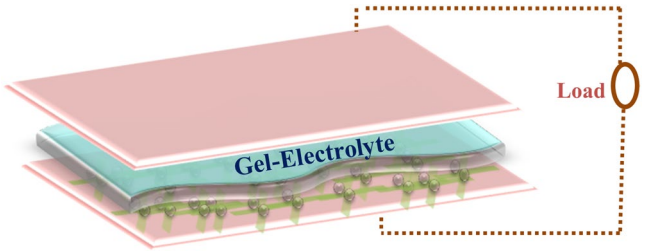

Figure 8. Schematic illustration of assembled g-C_3N_4@$ZnCo_2O_4$//g-C_3N_4@$ZnCo_2O_4$ symmetric supercapattery device using gel electrolyte.

maintained an energy efficiency of 75% in addition to a capacity retention of 71% up to 10000 continuous cycles at 15 Ag^{-1} as shown in Fig. 10(b). This demonstrates long-term electrochemical stability of the symmetric device. To further assess the electrochemical properties of device, the EIS analysis in Fig. 10(c) shows the solution resistance (R_s) before and after 10000 cycles of GCD. In the high-frequency region, R_s is the intercept on the Z'-axis, which is a combination of resistance in the electrolyte and the material electrode[30]. The calculated value of R_s before and after 10000 cycles is estimated to be 1.1 and 1.5 Ω, respectively, representing the stability of the synthesised material for fabricated supercapattery device. Moreover, the Nyquist plot for g-C_3N_4@$ZnCo_2O_4$//gel electrolyte//g-C_3N_4@$ZnCo_2O_4$ symmetric device was fitted as shown in Fig. 10(d) with its corresponding equivalent circuit displayed in the inset.

Experimental

Synthesis of the g-C_3N_4@$ZnCo_2O_4$ composite. All the reagents were of analytical quality and used without additional refinement. The g-C_3N_4 was prepared through simple pyrolysis of urea under ambient atmosphere. Initially, urea was dried at 80 °C for 24 hours and it was placed in a crucible for heat treatment in an oven. After heating the precursor at 550 °C for 3 hours, g-C_3N_4 of yellow-coloured was obtained. Then, 1 mM of Zinc Nitrate, 2 mM of Cobalt Nitrate and 5 mM of urea was dissolved properly in 40 mL deionized (DI) water by stirred for 30 min. The prepared 10 mg of the obtained g-C_3N_4 was then mixed with the prepared solution and stirred

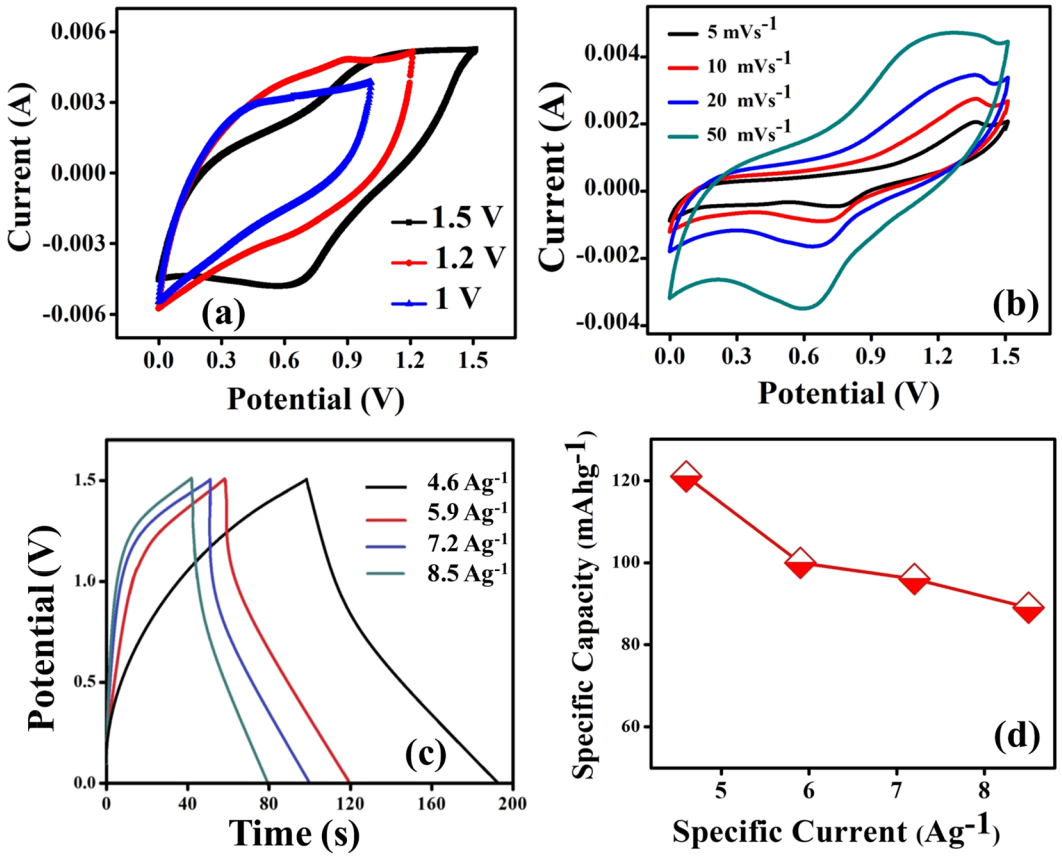

Figure 9. (**a**) CV curves of the g-C_3N_4@$ZnCo_2O_4$//gel electrolyte//g-C_3N_4@$ZnCo_2O_4$ symmetric supercapattery device measured at different potential windows. (**b**) CV curves of the g-C_3N_4@$ZnCo_2O_4$//gel electrolyte//g-C_3N_4@$ZnCo_2O_4$ measured at different scan rates ranging from 5 to 50 mVs^{-1} within the potential window of 0 to 1.5 V. (**c**) Galvanostatic charge-discharge curves of g-C_3N_4@$ZnCo_2O_4$//gel electrolyte//g-C_3N_4@$ZnCo_2O_4$ device at various specific current values. (**d**) Specific capacity as a function of specific current for g-C_3N_4@$ZnCo_2O_4$//gel electrolyte//g-C_3N_4@$ZnCo_2O_4$ device.

firmly for an additional 1 h. Then the entire solution was moved to a 70 mL Teflon-lined autoclave box and heated to 180 °C for 12 h. After the autoclave box was cooled to room temperature, the precursor was collected, rinsed consecutively with DI wand ethanol. Afterwards, the final product was calcinated at 450 °C for 2 h.

Electrochemical analysis of electrode and symmetric device. To fabricate the working electrodes, 80 wt% of as-synthesized g-C_3N_4@$ZnCo_2O_4$, 10 wt%) of carbon black and a polymer binder (polyvinylidene fluoride; PVDF, 10 wt%) was mixed using few drops of N-Methyl-2-pyrrolidone (NMP). The resulting slurry was applied on a flexible nickel mesh substrate (current collector) using the drop-casting method, followed by drying it at 120 °C for 12 h in an oven. The electrochemical measurements of electrodes were carried out on Biologic potentiostat workstation in a 6 M KOH electrolyte using cyclic voltammetry (CV), galvanostatic charge-discharge (GCD) and electrochemical impedance spectroscopy (EIS) measurements. In three electrodes configurations, the as-prepared electrode was used as a working electrode, Ag/AgCl and platinum were used as reference electrode and counter electrode, respectively.

The specific discharge capacity, Q_s ($mAhg^{-1}$) and energy efficiency, η(%) of electrodes was calculated from galvanostatic charge-discharge measurements by using the following equation

$$Q_S = \frac{I\Delta t}{3.6\ m} \tag{1}$$

$$\eta_E = \frac{E_d \times 100}{E_c} \tag{2}$$

where I represent discharge current, Δt is the discharge time taken to complete the discharge cycle, m is the active mass of the electrode. η_E is energy efficiency, E_d and E_c represents the charge and discharges energy[31].

The assembling of the symmetric device has been done using gel electrolyte (PVA/KOH), which works both as an electrolyte and a separator. To prepare the gel polymer electrolyte, 6 g of PVA was added to 6 M solution of

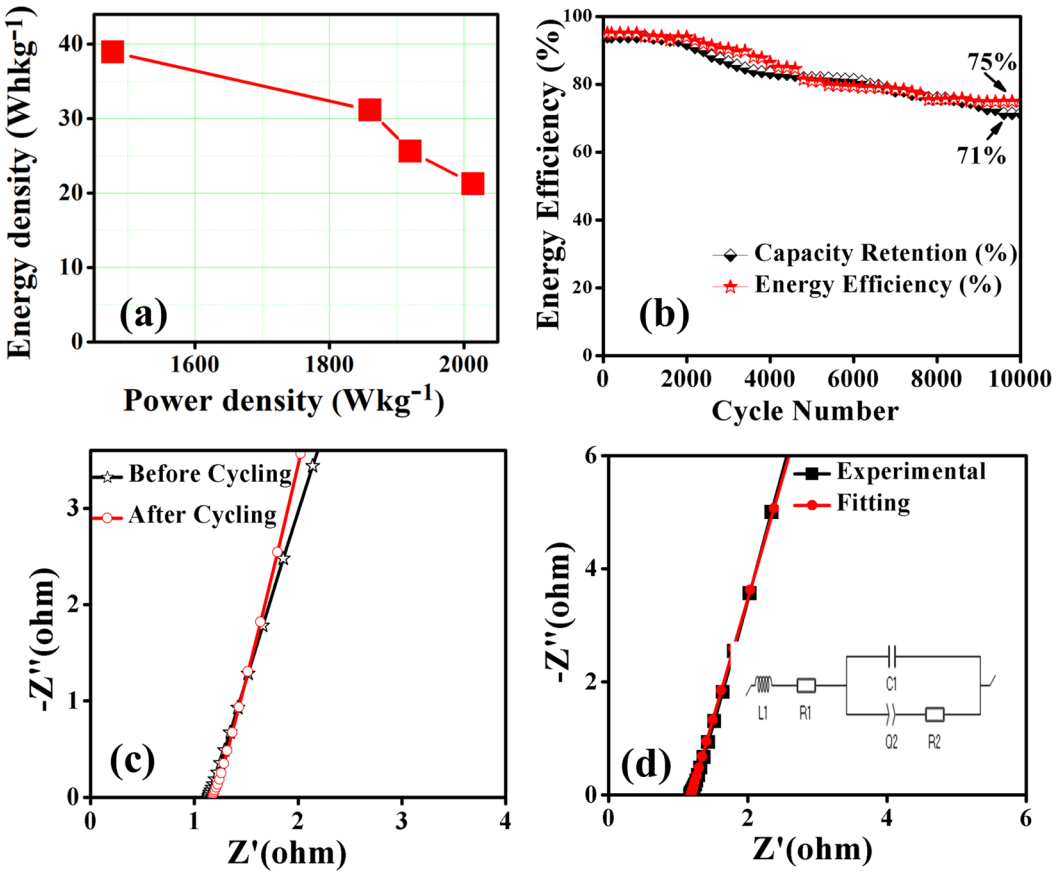

Figure 10. (**a**) Ragone plot for g-C_3N_4@$ZnCo_2O_4$//gel electrolyte//g-C_3N_4@$ZnCo_2O_4$ symmetric device. (**b**) Capacity retention and energy efficiency of g-C_3N_4@$ZnCo_2O_4$//gel electrolyte//g-C_3N_4@$ZnCo_2O_4$ symmetric device for 10000 cycles at 15 Ag^{-1}. (**c**) Nyquist impedance plot of g-C_3N_4@$ZnCo_2O_4$//gel electrolyte//g-C_3N_4@$ZnCo_2O_4$ symmetric device before and after cycling. (**d**) Fitted Nyquist plot of g-C_3N_4@$ZnCo_2O_4$//gel electrolyte//g-C_3N_4@$ZnCo_2O_4$ symmetric device and the equivalent circuit (insert).

KOH and then heating at 95 °C followed by firmly stirring for 2 h. To assemble a solid-state symmetric device, the gel electrolyte membrane was sandwiched between the two as-fabricated g-C_3N_4@$ZnCo_2O_4$ electrodes. The specific discharge capacity (Q_s) of symmetric device calculated from the GCD curves according to Eq. 1, where m is the total mass of active materials on both electrodes of the assembled device. The energy density (*Ed*) and power density (P_d) of the symmetric device is calculated using the following equations[32,33].

$$E_d = \frac{I}{3.6\,m}\int V dt \tag{3}$$

$$P_d = \frac{E_d \times 3600}{\Delta t} \tag{4}$$

where *I* describe the discharge current, *m* represents the mass of active material, the integral term is the area under the CD curve and Δt is the discharge time (seconds).

Characterization techniques. The phase and structure of the samples were investigated by X-ray powder diffraction (XRD) diffractometer with radiation of Cu Kα (λ = 0.15405 nm). The surface morphology of samples was characterized by scanning electron microscope (SEM, JEOL JSM-6390LV, 20 kV). To study the elemental composition of synthesized samples X-ray energy dispersive analyzer was used. The Brunauer-Emmett- Teller (BET) measurements were used to calculate the specific surface area and pore size distributions, performed on a Belsorp Max system using nitrogen gas adsorption/desorption isotherms.

Conclusions

We have developed a g-C_3N_4 supported $ZnCo_2O_4$ composite electrode using a simple hydrothermal method for improving the electrochemical performance of the electrode. The synergistic effect of g-C_3N_4 and $ZnCo_2O_4$ in g-C_3N_4@$ZnCo_2O_4$ hybrid composite shows a significant increase in a specific surface area along with a specific discharge capacity of 157 $mAhg^{-1}$. Accordingly, g-C_3N_4@$ZnCo_2O_4$//gel electrolyte//g-C_3N_4@$ZnCo_2O_4$ symmetric supercapattery device is fabricated, which displays a high specific discharge capacity of 121 $mAhg^{-1}$ at 4.6

Ag^{-1}. The device exhibits the highest energy density of 39 $Whkg^{-1}$ at a power density of 1478 Wkg^{-1}. A good cycling stability performance with an energy efficiency of 75% is observed up to 10,000 cycles. This novel strategy establishes a stage towards the construction of a hybrid electrode with prominent performance, which is the present demand for energy storage devices.

Received: 20 September 2019; Accepted: 2 January 2020;
Published online: 06 February 2020

References

1. Peng, L. *et al*. Ultrathin two-dimensional MnO_2/graphene hybrid nanostructures for high-performance, flexible planar supercapacitors. *Nano Lett.* **13**, 2151–2157 (2013).
2. Sanliang, Z. & Pan, N. Supercapacitors performance evaluation. Advanced Energy. *Materials* **5**, 1401401 (2015).
3. Lu, X. *et al*. Oxygen-deficient hematite nanorods as high-performance and novel negative electrodes for flexible asymmetric supercapacitors. *Adv. Mater.* **26**, 3148–3155 (2014).
4. Yury, G. & Simon, P. True performance metrics in electrochemical energy storage. *Science* **334**, 917–918 (2011).
5. Sundriyal, S., Sharma, M., Kaur, A., Mishra, S. & Deep, A. Improved electrochemical performance of rGO/TiO_2 nanosheet composite based electrode for supercapacitor applications. *J. Mater. Sci. Mater. Electron.* **29**, 12754–12764 (2018).
6. Oyedotun, K. O. *et al*. Synthesis of ternary NiCo-MnO_2 nanocomposite and its application as a novel high energy supercapattery device. *Chemical Engineering Journal* **335**, 416–433 (2018).
7. Tahir, M. *et al*. Multifunctional g-C_3N_4 nanofibers: A template-free fabrication and enhanced optical, electrochemical, and photocatalyst properties. *ACS Appl. Mater. Interfaces*, **6** 1258–1265 (2014).
8. Wei, B. *et al*. One-step synthesis of graphitic-C_3N_4/ZnS composites for enhanced supercapacitor performance. *J. Energy Chem.* **27**, 472–477 (2018).
9. Dong, B. *et al*. Formation of g-C_3N_4@$Ni(OH)_2$ Honeycomb Nanostructure and Asymmetric Supercapacitor with High Energy and Power Density. *ACS Appl. Mater. Interfaces*, **9** 17890–17896 (2017).
10. Li, L. *et al*. $Ni(OH)_2$ nanosheets grown on porous hybrid g-C_3N_4/RGO network as high-performance supercapacitor electrode. *Sci. Rep.* **7**, 43413 (2017).
11. Chang, X. *et al*. MnO_2/g-C_3N_4 nanocomposite with highly enhanced supercapacitor performance. *Nanotechnology* **28**, 135705 (2017).
12. Guo, W. *et al*. A Novel CVD Growth of g-C_3N_4 Ultrathin Film on $NiCo_2O_4$ Nanoneedles/Carbon Cloth as Integrated Electrodes for Supercapacitors. *ChemElectroChem* **5**, 3383–3390 (2018).
13. Chen, T. *et al*. All-solid-state high-performance asymmetric supercapacitors based on novel MnS nanocrystal and activated carbon materials. *Sci. Rep.* **6**, 23289 (2016).
14. Liu, B. *et al*. New energy storage option: Toward $ZnCo_2O_4$ nanorods/nickel foam architectures for high-performance supercapacitors. *ACS Appl. Mater. Interfaces* **5**, 10011–10017 (2013).
15. Zhao, C. *et al*. One-step hydrothermal preparation of TiO_2/RGO/$Ni(OH)_2$/NF electrode with high performance for supercapacitors. Electrochim. *Acta* **218**, 216–227 (2016).
16. Shi, Y. *et al*. Enhanced thermal stability of polystyrene by graphitic carbon nitride/spinel $ZnCo_2O_4$ nanohybrids and the catalytic mechanism investigation. *RSC Adv.* **5**, 41835–41838 (2015).
17. Sharma, M., Sundriyal, S., Panwar, A. K. & Gaur, A. Facile synthesis and electrochemical performance of Mg-substituted $Ni_{1-x}MgxCo_2O_4$ mesoporous nanoflakes for energy storage applications. *Electrochim. Acta* **294**, 53–59 (2019).
18. Pendashteh, A. *et al*. Highly Ordered Mesoporous $CuCo_2O_4$ Nanowires, a Promising Solution for High-Performance Supercapacitors. *Chem. Mater.* **27**, 3919–3926 (2015).
19. Vijayakumar, S., Nagamuthu, S., Lee, S.-H. & Ryu, K.-S. Porous thin layered nanosheets assembled $ZnCo_2O_4$ grown on Ni-foam as an efficient electrode material for hybrid supercapacitor applications. *Int. J. Hydrogen Energy* **42**, 3122–3129 (2017).
20. Li, M., Ma, K. Y., Cheng, J. P., Lv, D. & Zhang, X. B. Nickel-cobalt hydroxide nanoflakes conformal coating on carbon nanotubes as a supercapacitive material with high-rate capability. *J. Power Sources* **286**, 438–444 (2015).
21. Sharma, M., Sundriyal, S., Panwar, A. & Gaur, A. Enhanced supercapacitive performance of $Ni_{0.5}Mg_{0.5}Co_2O_4$ flowers and rods as an electrode material for high energy density supercapacitors: Rod morphology holds the key. *J. Alloys Compd.* **766**, 859–867 (2018).
22. Laheäär, A., Przygocki, P., Abbas, Q. & Béguin, F. Appropriate methods for evaluating the efficiency and capacitive behaviour of different types of supercapacitors. *Electrochemistry Communications* **60**, 21–25 (2015).
23. Jadhav, H. S., Pawar, S. M., Jadhav, A. H., Thorat, G. M. & Seo, J. G. Hierarchical Mesoporous 3D Flower-like $CuCo_2O_4$/NF for High-Performance Electrochemical Energy Storage. *Sci. Rep.* **6**, 31120 (2016).
24. Tang, H. *et al*. Growth of polypyrrole ultrathin films on mos_2 monolayers as high-performance supercapacitor electrodes. *Adv. Mater.* **27**, 1117–1123 (2015).
25. Chodankar, N. R., Dubal, D. P., Gund, G. S. & Lokhande, C. D. A symmetric MnO_2/MnO_2 flexible solid state supercapacitor operating at 1.6V with aqueous gel electrolyte. *J. Energy Chem.* **25**, 463–471 (2016).
26. Zhou, S. *et al*. Designed formation of Co_3O_4/$ZnCo_2O_4$/CuO hollow polyhedral nanocages derived from zeolitic imidazolate framework-67 for high-performance supercapacitors. *Nanoscale* **10**, 15771–15781 (2018).
27. Zhu, J. *et al*. Two-dimensional porous $ZnCo_2O_4$ thin sheets assembled by 3D nanoflake array with enhanced performance for aqueous asymmetric supercapacitor. *Chem. Eng. J.* **336**, 679–689 (2018).
28. Gao, Z. *et al*. $ZnCo_2O_4$-reduced graphene oxide composite with balanced capacitive performance in asymmetric supercapacitors. *Appl. Surf. Sci.* **442**, 138–147 (2018).
29. Sahoo, S. & Shim, J. J. Facile Synthesis of Three-Dimensional Ternary $ZnCo_2O_4$/Reduced Graphene Oxide/NiO Composite Film on Nickel Foam for Next Generation Supercapacitor Electrodes. ACS Sustain. *Chem. Eng.* **5**, 241–251 (2017).
30. Syed, J. A., Ma, J., Zhu, B., Tang, S. & Meng, X. Hierarchical Multicomponent Electrode with Interlaced $Ni(OH)_2$ Nanoflakes Wrapped Zinc Cobalt Sulfide Nanotube Arrays for Sustainable High-Performance Supercapacitors. *Adv. Energy Mater.* **7**, 1701228 (2017).
31. Oyedotun, K. O. *et al*. Electrochemical performance of two-dimensional Ti_3C_2-Mn_3O_4 nanocomposites and carbonized iron cations for hybrid supercapacitor electrodes. *Electrochimica Acta*. **301**, 487–499 (2019).
32. Liu, J., Zhang, T., Wang, Z., Dawson, G. & Chen, W. Simple pyrolysis of urea into graphitic carbon nitride with recyclable adsorption and photocatalytic activity. *J. Mater. Chem.* **21**, 14398–14401 (2011).
33. Shao, Y. *et al*. Graphene-based materials for flexible supercapacitors. *Chem. Soc. Rev.* **44**, 3639–3665 (2015).

Acknowledgements

One of the authors, Ms Meenu Sharma, thanks to Director, N.I.T Kurukshetra to provide the MHRD fellowship research facilities to accomplish this work. One of the authors, Anurag Gaur, is thankful to Science and Engineering Research Board (SERB), Govt. of India for providing funding through research project No: CRG/2018/001694. Authors also acknowledge Dr. AkashDeep and Dr. Sunita Mishra from CSIO, Chandigarh for providing BET facility.

Author contributions

M. Sharma is the Ph.D student, who performed the experimental measurements. Dr. Anurag Gaur is the Ph.D advisor, who contributed in the data analysis and writing the manuscript.

Competing interests

The authors declare no competing interests.

Additional information

Supplementary information is available for this paper at https://doi.org/10.1038/s41598-020-58925-4.

Correspondence and requests for materials should be addressed to A.G.

Reprints and permissions information is available at www.nature.com/reprints.

Publisher's note Springer Nature remains neutral with regard to jurisdictional claims in published maps and institutional affiliations.